

## Supplementary Information

### Disease-associated missense mutations in the GluN2B subunit alter NMDA receptor ligand binding and ion channel properties

Laura Fedele<sup>1,2</sup>, Joseph Newcombe<sup>3</sup>, Maya Topf<sup>3</sup>, Alasdair Gibb<sup>2</sup>,  
Robert J Harvey<sup>4,5\*</sup> & Trevor G Smart<sup>2\*</sup>

#### Supplementary Note 1

The following calculation shows how we converted Hartree units (Ha) (atomic units of energy) into binding energy (kcal/mol) for Mg<sup>2+</sup> interacting with its binding site in the NMDAR channel. Note 1 Ha = 627.509 kcal/mol.

For the coordination of Mg<sup>2+</sup> by the NMDAR channel asparagines, we calculated the following energies at 298.15 K:

For the octahedral coordination of Mg<sup>2+</sup> by 6 waters = -1490.865140 Ha

For the 4 asparagine residues alone = -658.509131 Ha

For a single water molecule = -76.426767 Ha.

And for Mg<sup>2+</sup> coordinated by the 4 asparagines and 2 water molecules = -1843.68261 Ha.

By substituting these Ha values into the following equation we obtain the binding energy of Mg<sup>2+</sup> coordinated by the asparagines:



$$-1843.68261 + 4 \times (-76.426767) - (-658.509131) - (-1490.865140) = -0.015407 \text{ Ha}$$

This can be converted to kcal/mol as follows:

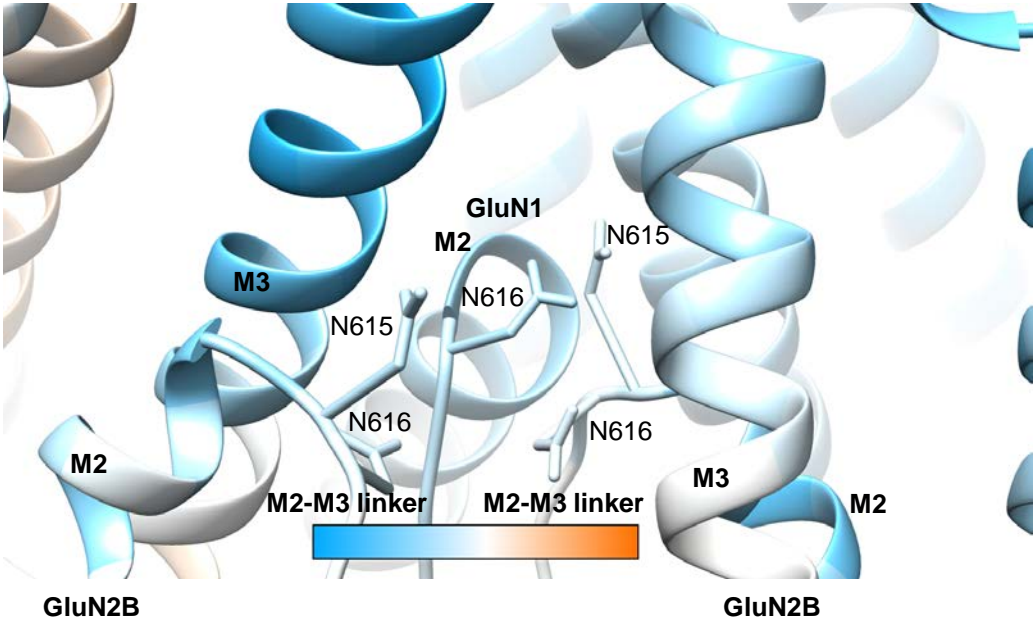
$$-0.015407 \times 627.51 = -9.668047 \text{ kcal/mol.}$$

This value represents the theoretical  $\Delta G$  for binding for  $Mg^{2+}$  to the 4 asparagines.

This value is also comparable to  $\Delta G$  calculated from the trapping model for the wild-type GluN1-GluN2B which is -3.95 kcal/mol. This value was determined for  $Mg^{2+}$  coordination in the presence of permeant ions,  $Na^+$ ,  $K^+$  and  $Ca^{2+}$ . The  $\Delta G$  from the trapping model was calculated from;  $\Delta G = RT \ln K$ , where  $K$  is the  $Mg^{2+}$ (0 mV) dissociation constant taken from Table 2,  $R = 1.987 \text{ cal.mol}^{-1}.\text{K}^{-1}$ , and  $T = 293 \text{ K}$ .

## **Supplementary Figures and Tables**

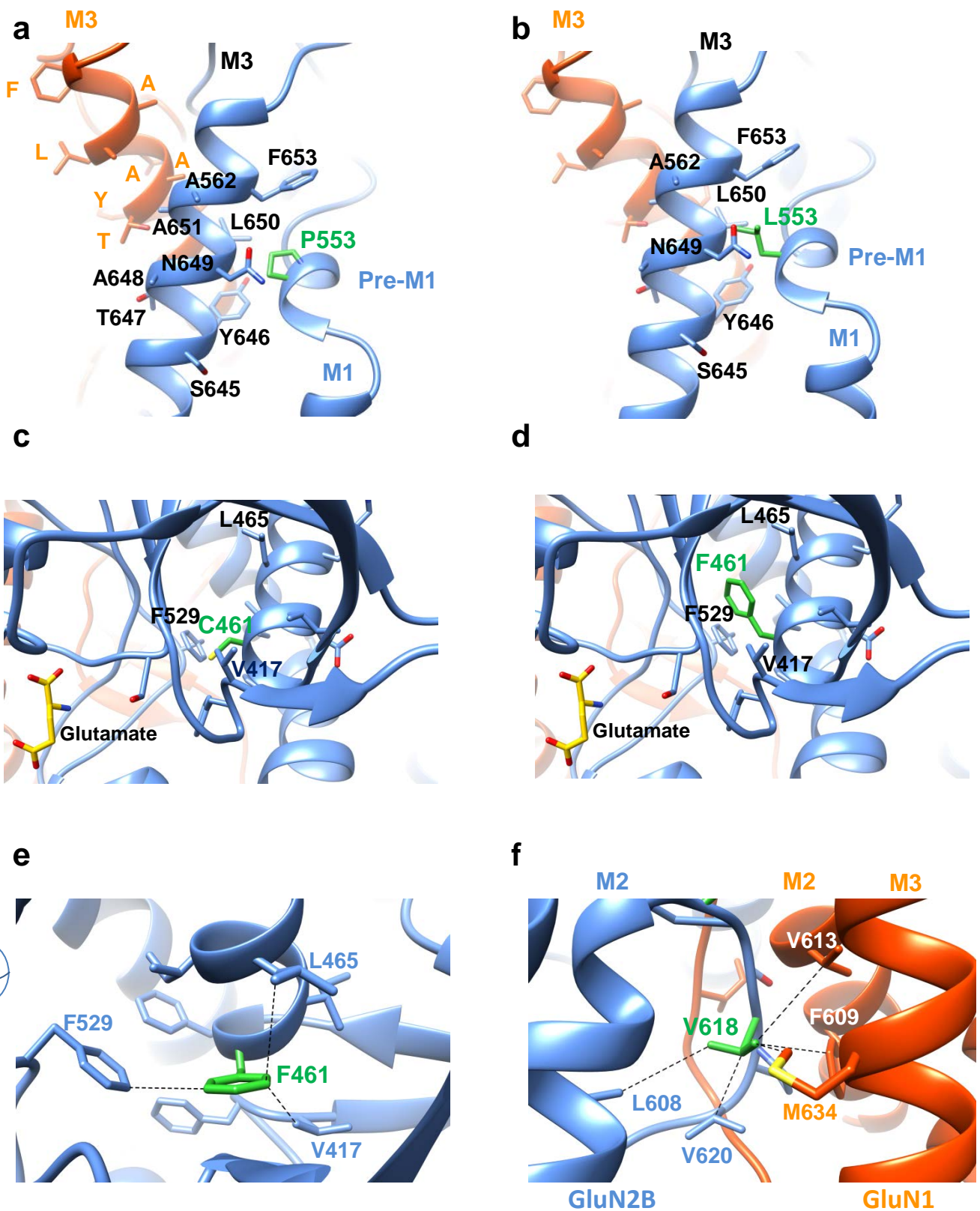
Supplementary Fig 1. Aligning the pore region for GluN1-GluN2B



### **Supplementary Figure 1. Aligning the pore region for GluN1-GluN2B tetramers**

The TMD including the pore region of the GluN2B subunit is subjected to a root-mean-standard deviation (RMSD) analysis between the C $\alpha$  of our human NMDAR model and the *Xenopus* NMDAR PDB 4TLM. RMSD bar: blue = 0 ('good fit'), white = 5, orange = 10. For simplicity only three subunits are shown.

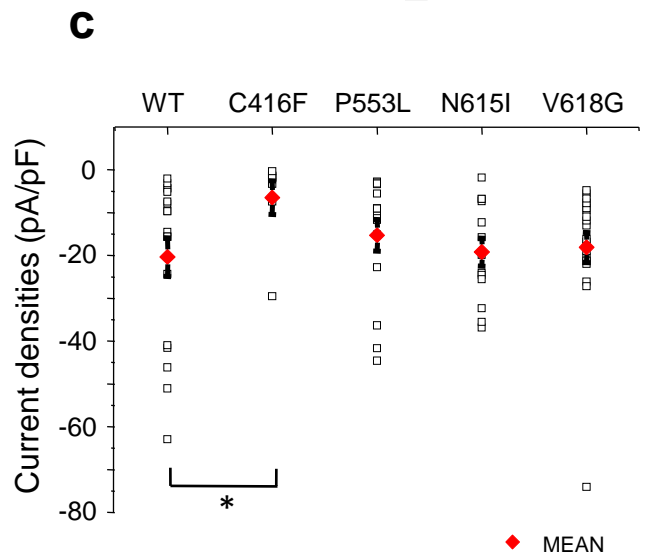
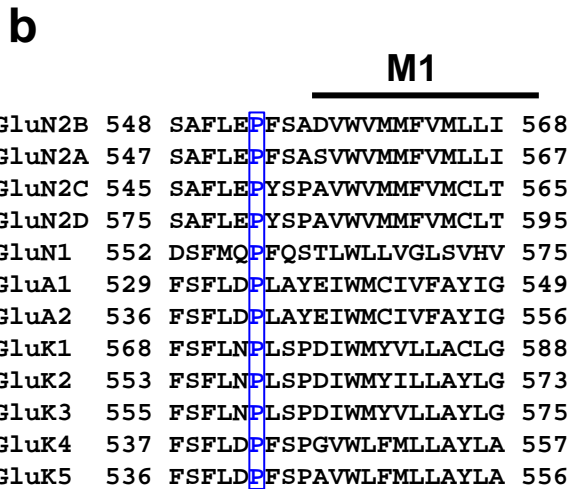
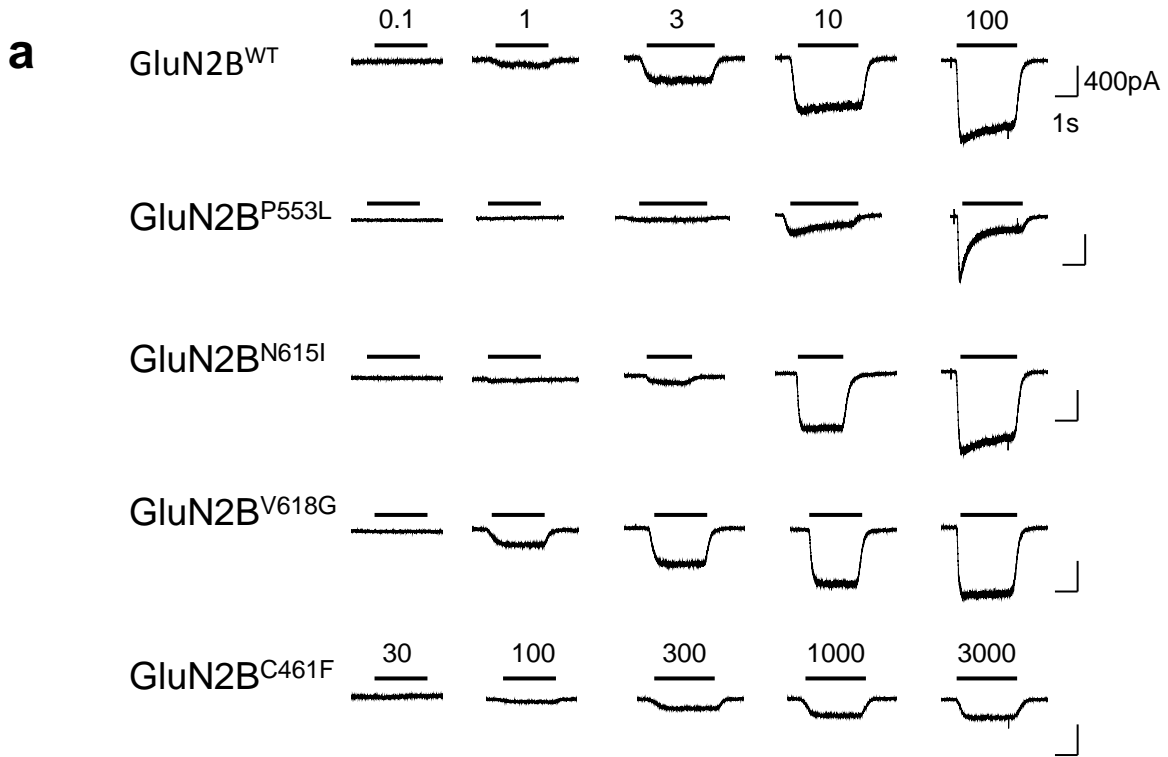
Supplementary Fig 2: Locations and interactions of GluN2B missense mutations in the human NMDAR model



**Supplementary Figure 2. Locations and interactions of GluN2B missense mutations in the human NMDAR model.**

(a) P553 is located in pre-M1, close to the –SYTANLAAF- motif (black, numbered amino acids shown) in M3 of the same subunit, which is also juxtaposed to the –SYTANLAAF- motif in M3 from the adjacent GluN1 subunit (orange, amino acids shown in single letter format). (b) The P553L substitution may disrupt receptor gating via interactions between L553 and N649 and/or L650 of the –SYTANLAAF- motif (1.7Å and 3.4Å). (c-e) C461 is located in the S1 domain of the LBD, but is not involved in the direct binding of glutamate. The C461F substitution could engage in van-der-Waal interactions with neighbouring residues in S1 of the same subunit (e.g., V417 and L465) or aromatic interactions with the neighbouring F529. The distance between F461 and the three neighbouring residues is ~5Å. Note change in the viewing angle from d to e. (f) V618, located in the ion channel, interacts with neighbouring hydrophobic residues via van der Waal interactions: L608 (in M2 of GluN2B, 4.8Å), V602 (in M2-M3 linker of GluN2B, 3.8Å), F609 (in M1 of GluN1, 4.1Å), M634 (in M3 of GluN1; 4.3Å) and V613 (in M2 of GluN1, 5.0Å).

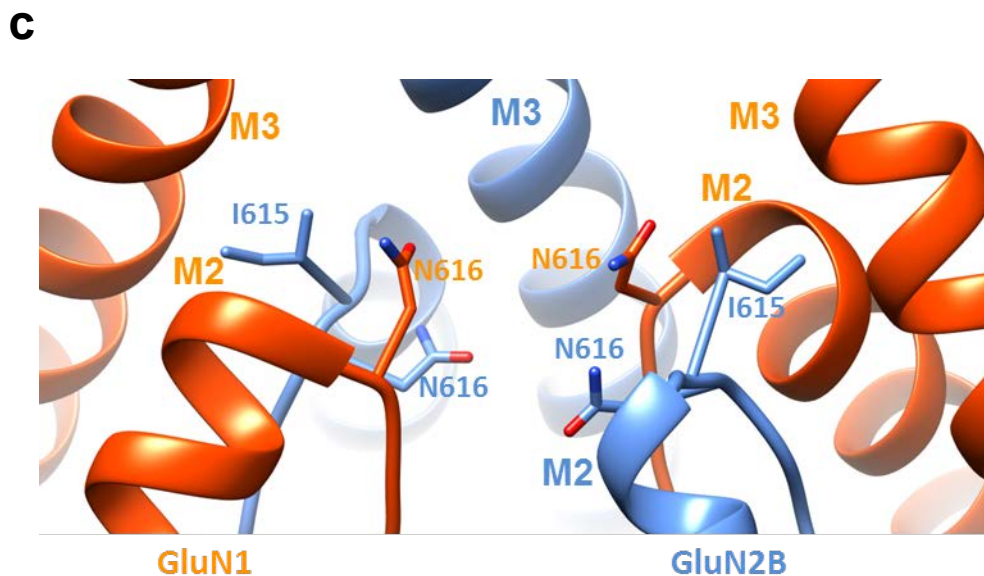
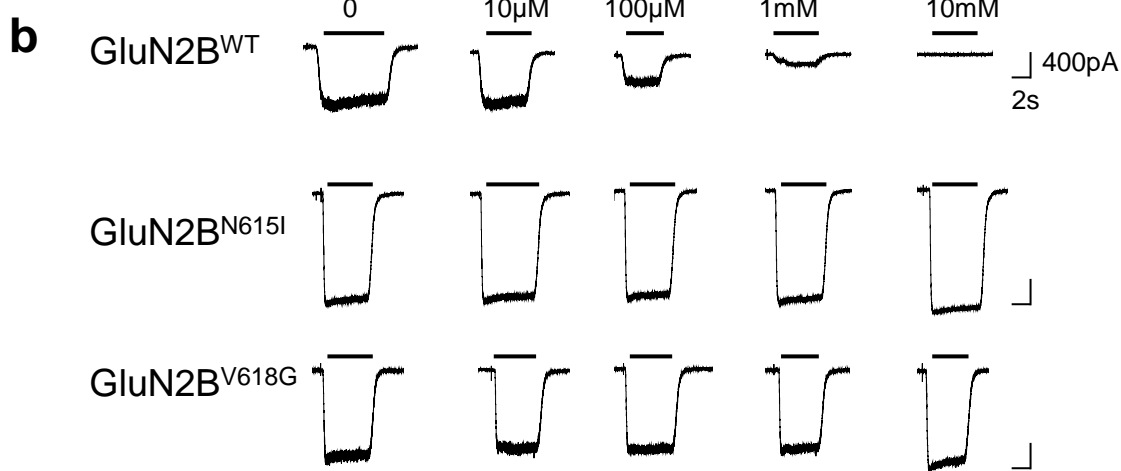
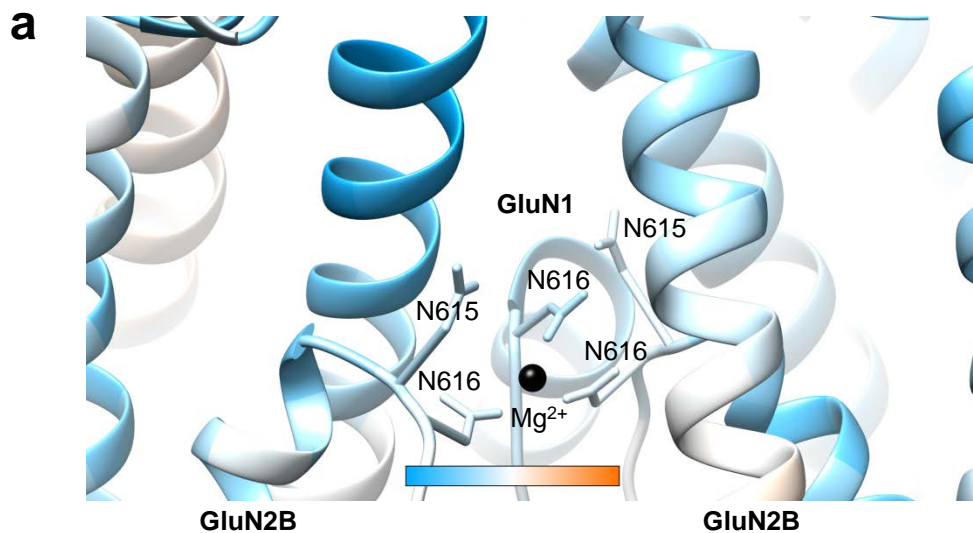
# Supplementary Fig. 3 Glutamate sensitivity of GluN2B mutants



### Supplementary Figure 3. Glutamate sensitivity of GluN2B mutants

(a) Membrane currents activated by a range of glutamate concentrations co-applied with 10  $\mu$ M glycine in wild-type (WT) GluN1-GluN2B receptors and C461F, P553L, N615I or V618G GluN2B mutants. Cells were voltage clamped at -30 mV. (b) Primary sequence alignment for human ionotropic GluRs in pre-M1. P553 in GluN2B (blue, boxed) is highly conserved across the receptor family. (c) Current densities determined from whole-cell recording from HEK293 cells expressing WT and mutant GluN1-GluN2B NMDARs. Individual membrane currents elicited by saturating glutamate concentrations (-30 mV) were normalised to the cell capacitance. Mean values are shown by a red diamond. GluN2B<sup>WT</sup>:  $-20.36 \pm 4.54$  pA/pF (n = 18); GluN2B<sup>C461F</sup>:  $-6.49 \pm 3.94$  (n = 7); GluN2B<sup>P553L</sup>:  $-15.31 \pm 3.70$  (n = 15); GluN2B<sup>N615I</sup>:  $-19.19 \pm 3.24$  (n = 13); GluN2B<sup>V618G</sup>:  $-17.55 \pm 3.35$  (n = 20). Data analysed using a one-way ANOVA with Dunnett's post-hoc test, \* p < 0.05.

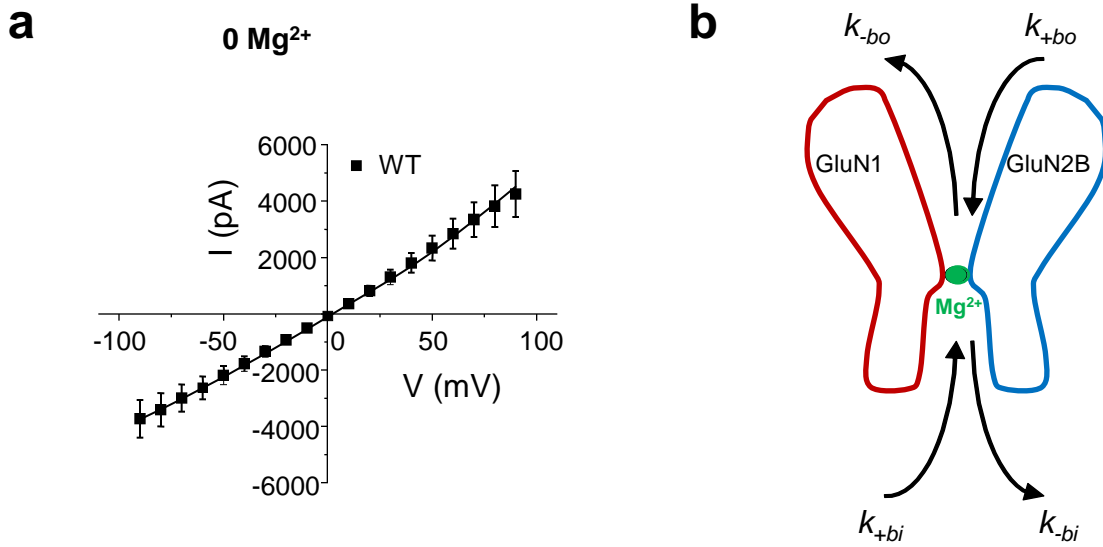
# Supplementary Fig 4. Mg<sup>2+</sup> coordination site and its disruption by NMDA channel mutants



#### **Supplementary Figure 4. Mg<sup>2+</sup> coordination site and its disruption by NMDA channel mutants**

(a) Root-mean-standard deviation (RMSD) analysis of the TMD between the C $\alpha$  of our human NMDAR model and the *Xenopus* PDB 4TLM reproduced from Supplementary Fig. 1. RMSD bar: blue= 0 ('good fit'), white= 5, orange= 10, black (unaligned regions). Here, Mg<sup>2+</sup> is included in the channel and shown as a black sphere. (b) Membrane currents elicited by 10  $\mu$ M glutamate and 10  $\mu$ M glycine at different Mg<sup>2+</sup> concentrations in HEK293 cells transfected with GluN1 and GluN2B subunits (WT, N615I or V618G) voltage clamped at -60 mV. GluN1-GluN2B<sup>WT</sup> receptors are inhibited by Mg<sup>2+</sup>, whereas GluN1-GluN2B<sup>N615I</sup> and GluN1-GluN2B<sup>V618G</sup> are insensitive to Mg<sup>2+</sup> block. Calibrations apply to all currents. (c) The N615I substitution disrupts H-bonding between GluN2B<sup>N615I</sup> and GluN1<sup>N616</sup>. These H-bonds are critical for stabilizing the coordination of Mg<sup>2+</sup> by the two sets of GluN1<sup>N616</sup> and GluN2B<sup>N616</sup> residues.

Supplementary Fig. 5 Trapping model applied to Mg<sup>2+</sup> block



**c** Mg<sup>2+</sup> binding association and dissociation factors

	$k_{+bo}$ (0mV) (M <sup>-1</sup> s <sup>-1</sup> )	$k_{-bo}$ (0mV) s <sup>-1</sup>	$k_{+bi}$ (0mV) (M <sup>-1</sup> s <sup>-1</sup> )	$k_{-bi}$ (0mV) s <sup>-1</sup>	$K_{Mg}$ (0mV)
<b>WT</b>	$5 \times 10^7$	24686	$5 \times 10^7$	25124	1.07 mM
<b>N615I</b>	$5 \times 10^7$	$10^6$	$0.9 \times 10^6$	$0.9 \times 10^6$	> 1 M
<b>V618G</b>	$5 \times 10^7$	$1 \times 10^7$	$5 \times 10^7$	$2.41 \times 10^6$	123 mM

**d** Ion permeation rates

	Na <sup>+</sup> /K <sup>+</sup>			Ca <sup>2+</sup>		
	$k_{+bo}$ (0mV) (M <sup>-1</sup> s <sup>-1</sup> )	$k_{-bo}$ (0mV) s <sup>-1</sup>	$k_{-bi}$ (0mV) (s <sup>-1</sup> )	$k_{+bo}$ (0mV) (M <sup>-1</sup> s <sup>-1</sup> )	$k_{-bo}$ (0mV) s <sup>-1</sup>	$k_{-bi}$ (0mV) (s <sup>-1</sup> )
<b>WT</b>	$7.5 \times 10^8$	$6.8 \times 10^8$	$2 \times 10^8$	$5 \times 10^8$	$2 \times 10^6$	$2 \times 10^6$
<b>N615I</b>	$7.5 \times 10^8$	$1 \times 10^8$	$3.8 \times 10^7$	$2 \times 10^8$	$1 \times 10^5$	$2.5 \times 10^5$
<b>V618G</b>	$7.5 \times 10^8$	$8.3 \times 10^6$	$1.8 \times 10^7$	$2 \times 10^8$	$1 \times 10^5$	$1.7 \times 10^7$

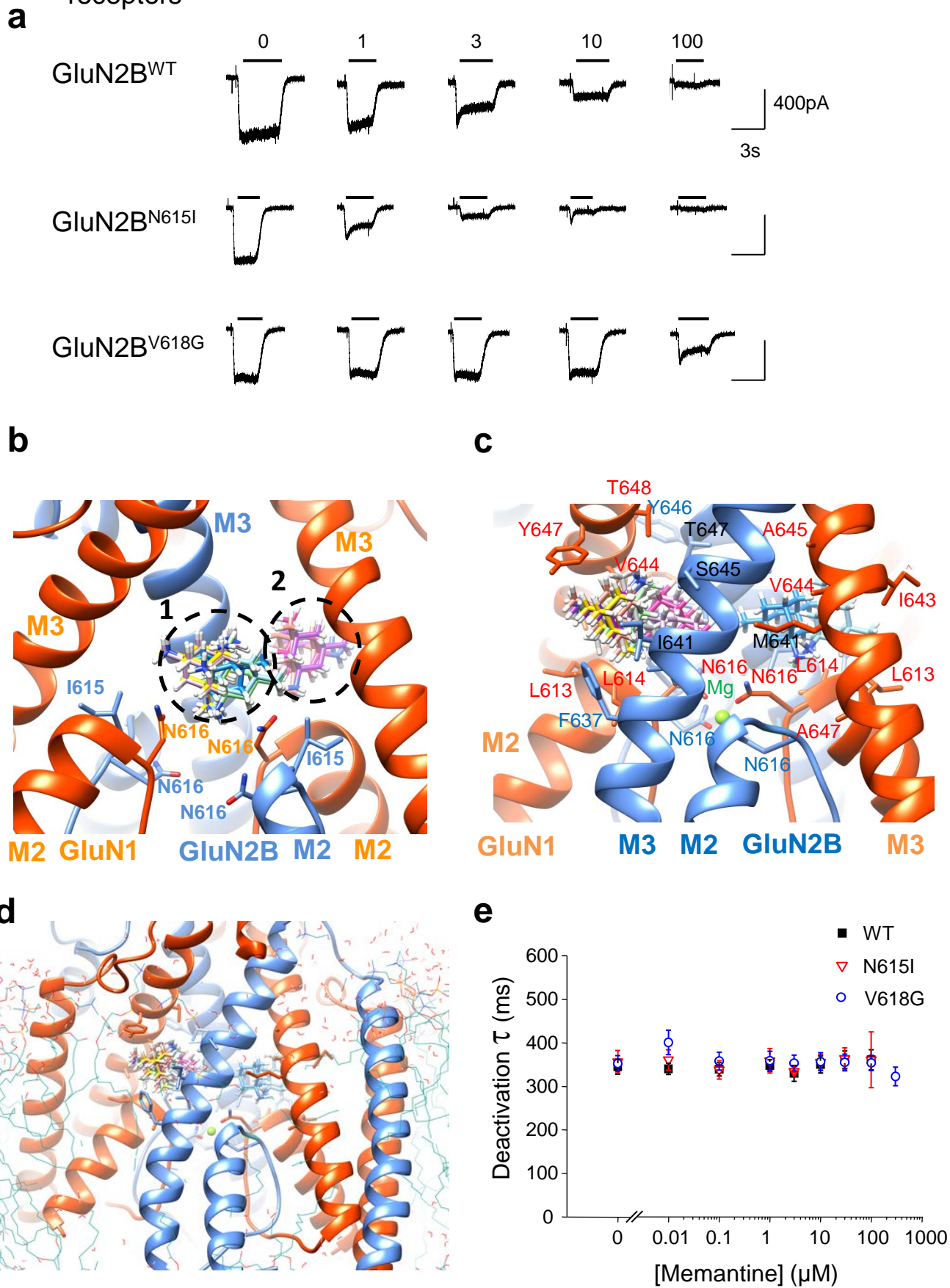
**e** I-V relationships with Mg<sup>2+</sup> and memantine

	External 0 mM Mg <sup>2+</sup>				External 1.2 mM Mg <sup>2+</sup>					
	10μM Glu		10μM Glu + 30μM Mem		10μM Glu		10μM Glu+ 30μM Mem		10μM Glu + 300μM Mem	
	N	V <sub>rev</sub>	N	V <sub>rev</sub>	N	V <sub>rev</sub>	N	V <sub>rev</sub>	N	V <sub>rev</sub>
<b>WT</b>	14247	1.75	11424	3.96	11735	6.69	14780	4.96	-	-
<b>N615I</b>	-	-	-	-	12372	-1.63	15069	7.54	-	-
<b>V618G</b>	-	-	-	-	9577	12.0	5569	12.04	5141	12.06

### Supplementary Figure 5. Trapping model applied to $Mg^{2+}$ block

(a) I-V relationships for GluN1-GluN2B<sup>WT</sup> in Krebs solutions with 0  $Mg^{2+}$  using a voltage step protocol (from -90 to +90 mV) elicited by 10  $\mu$ M glutamate and 10  $\mu$ M glycine in Krebs solution with nominally 0  $Mg^{2+}$ . Experimental data are shown as symbols (mean  $\pm$  s.e.m.), the curves were generated by the trapping model. (b) Schematic representation of  $Mg^{2+}$  binding in the NMDAR channel. A single  $Mg^{2+}$  ion can approach the binding site from either the inside (i) or outside (o) surface of the membrane with forward and backward rate constants  $k_{+b}$  and  $k_{-b}$  as indicated. (c) Table of predicted association and dissociation rate constants for  $Mg^{2+}$  binding and unbinding to the NMDAR channel. A single set of  $Mg^{2+}$  block and permeation rate constants consistent with the observed data for both wild-type and mutant receptors were used for both the trapping block model and permeation model. (d) Permeation model association rates for  $Na^+$  and  $K^+$  were constrained to be equal, while for  $Ca^{2+}$  permeation these rates were varied to allow matching of the currents in high calcium solution for wild-type, N615I and V618 mutant NMDARs. (e) Table of I-V relationship parameters for glutamate currents in the presence and absence of  $Mg^{2+}$  and/or memantine. These values were determined by fitting the trapping model to the experimental I-V data.

Supplementary Fig. 6. Memantine inhibition of GluN1-GluN2B receptors



## Supplementary Figure 6. Memantine inhibition of GluN1-GluN2B receptors

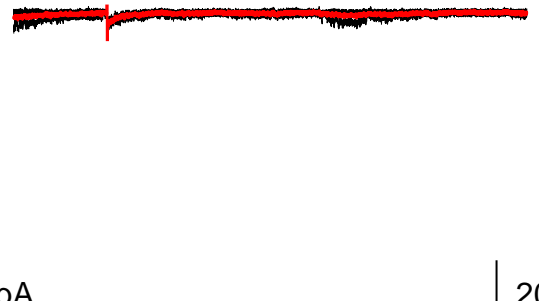
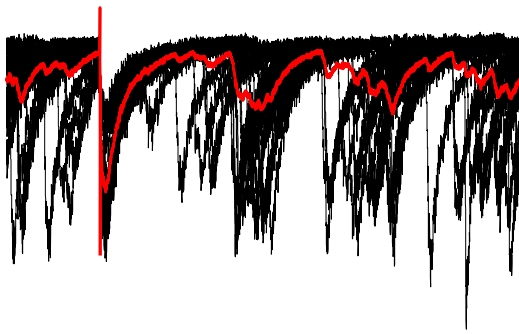
(a) Membrane currents elicited by 10  $\mu\text{M}$  glutamate and 10  $\mu\text{M}$  glycine at different memantine concentrations ( $\mu\text{M}$ ) in HEK293 cells (at -30 mV) expressing WT and mutant GluN1-GluN2B receptors. (b) Molecular docking of memantine in the GluN1-GluN2B<sup>N615I</sup> receptor results in two defined binding clusters: one cluster (pose 1) is located just above the channel pore (coincident with the binding position noted in the WT receptor, see Fig. 4); the other (pose 2) is characterised by displacement of memantine to a cavity between the M2 and M3 helices. (c) Memantine docking in a GluN1-GluN2B structure with bound  $\text{Mg}^{2+}$  *in situ*: the docked  $\text{Mg}^{2+}$  ion laterally displaces memantine from the preferred binding site (pose 1; the 10 highest ranked memantine poses are shown) that is characterised by hydrophobic residues. (d) The displaced binding site for memantine is shown in relation to the transmembrane domain. The lipid bilayer is present for illustrative purposes. The human GluN1-GluN2B receptor model was superimposed on the PDB 4TLM embedded in the plasma membrane from MEMprot (<http://memprotmd.bioch.ox.ac.uk/>). (e) Deactivation time constants ( $\tau$ ) determined with varying memantine concentrations. Decay kinetics were described by a single exponential following the removal of co-applied 10  $\mu\text{M}$  glutamate + 10  $\mu\text{M}$  glycine alone and with a range of memantine concentrations. Memantine did not affect deactivation time for GluN1-GluN2B<sup>WT</sup>, GluN1-GluN2B<sup>N615I</sup> and GluN1-GluN2B<sup>V618G</sup>.

Supplementary Fig. 7 Properties of evoked EPSCs

**a**

Control

+ 20  $\mu$ M APV



200pA  
1s

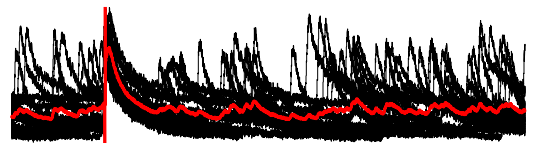
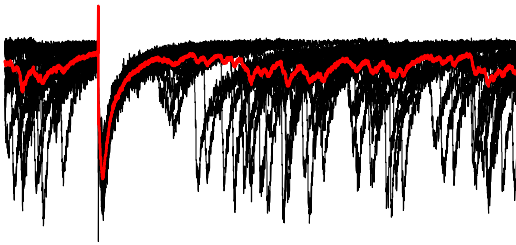
200pA  
1s

**b**

-70mV

+40mV

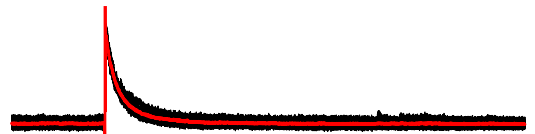
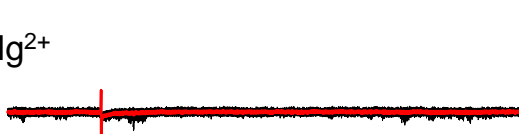
0  $Mg^{2+}$



200pA  
1s

200pA  
1s

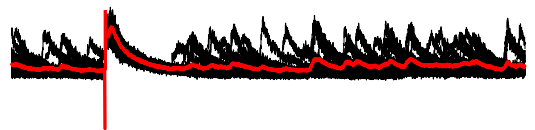
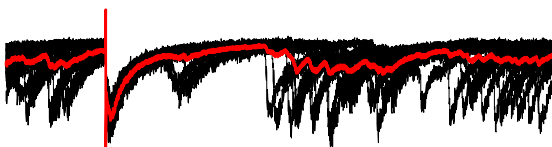
1.2mM  $Mg^{2+}$



200pA  
1s

200pA  
1s

0  $Mg^{2+}$



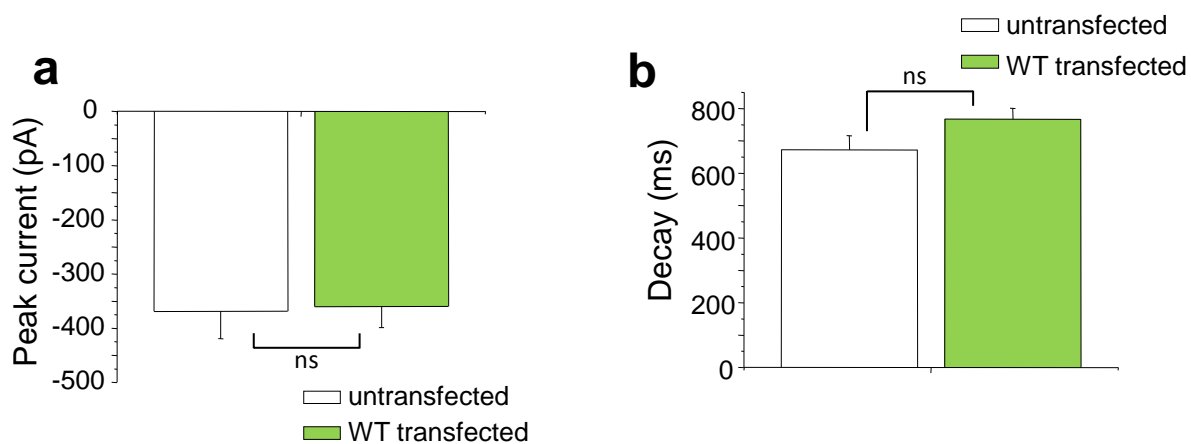
200pA  
1s

200pA  
1s

### **Supplementary Figure 7. Properties of evoked EPSCs**

(a) Evoked EPSCs ( $V_h$  -70 mV) in Krebs supplemented with 10  $\mu$ M CNQX, 20  $\mu$ M bicuculline and 10  $\mu$ M D-serine, are blocked by 20  $\mu$ M D-APV, indicating they are mediated by NMDARs. (b) Krebs containing 1.2 mM  $Mg^{2+}$  inhibits the evoked EPSCs at -70 mV holding potential but not at +40 mV, consistent with the  $Mg^{2+}$  voltage-dependent block of NMDARs. Upper paired traces: evoked EPSCs at -70 and +40 mV in 0  $Mg^{2+}$ ; middle traces: evoked EPSCs in 1.2 mM  $Mg^{2+}$  at the same holding potentials; lower traces: evoked EPSCs following re-perfusion with 0  $Mg^{2+}$  Krebs. Calibration values apply to all traces.

Supplementary Fig. 8. Comparison of evoked EPSCs between untransfected and wild-type GluN2B transfected neurons



**Supplementary Figure 8. Comparison of evoked EPSCs between untransfected and wild-type GluN2B transfected neurons**

(a) Bar graph comparing the mean peak EPSC amplitude between untransfected (DIV 13-16) and wild-type GluN2B cDNA transfected neurons (DIV 13-16). (b) Comparison of the mean EPSC weighted decay time constant for untransfected and wild-type GluN2B cDNA transfected neurons. Number of cells: untransfected; 19, transfected; 25.

Supplementary Table 1. Bioinformatic analyses of GluN2B missense mutations.

Residue	Phenotype	SIFT <sup>a</sup>	Polyphen-2 <sup>b</sup>	Mutation taster <sup>c</sup>	Ref
<b>L825V</b>	Autism	Tolerated: 0.12	Prob. damaging: 1.000	Disease causing	1
<b>A590T</b> * <sup>(1)</sup>	Phenotype?	Tolerated: 0.18	Prob.damaging: 0.987	Disease causing	2
<b>R682C</b>	Moderate ID	Damaging: 0	Prob.damaging: 1.000	Disease causing	
<b>A1267S</b> * <sup>(2)</sup>	Phenotype?	Tolerated: 0.45	Benign: 0.000	Polymorphism	
<b>M1331I</b> * (1)	Phenotype?	Tolerated: 0.2	Benign: 0.000	Disease causing	
<b>C461F</b>	LGS	Damaging: 0	Prob. damaging: 1.000	Disease causing	3
<b>A636P</b>	Mild ID	Damaging: 0	Prob. damaging: 1.000	Disease causing	4
<b>p.P553L</b>	Severe ID	Damaging: 0	Poss. damaging: 0.951	Disease causing	5
<b>p.C456Y</b>	Autism	Damaging: 0	Prob. damaging: 1.000	Disease causing	6
<b>p.V618G</b>	West syndrome	Damaging: 0	Prob. damaging: 1.000	Disease causing	7
<b>p.N615I</b>	West syndrome	Damaging: 0	Prob. damaging: 1.000	Disease causing	
<b>p.R540H</b>	West syndrome	Damaging: 0	Prob. damaging: 0.999	Disease causing	
<b>p.R1110C</b> * (1)	Phenotype?	Tolerated: 0.17	Prob. damaging: 0.998	Disease causing	8

## **Supplementary Table 1. Bioinformatics analyses of GluN2B missense mutations**

Data indicate the likelihood of GluN2B missense mutations causing disease as predicted by bioinformatics software. The scores indicate various categories of potential disease association: aSIFT: Damaging mutations are scores  $\leq 0.05$ ; Tolerated mutation =  $0.05 \leq \text{score} \leq 1$ ; bPolyphen-2: Probably damaging =  $0.957 \leq \text{score} \leq 1$ ; Possibly damaging =  $0.447 \leq \text{score} \leq 0.956$ ; Benign =  $\text{score} < 0.447$ ; cMutation Taster: mutations are either classified as: “polymorphism” or “disease causing”. For Phenotype, the ‘phenotype ?’ category is used when the citation does not explicitly denote the phenotype of the subject presenting the mutant. ID indicates intellectual disability; LGS is the Lennox-Gastaut syndrome. Amino acid substitutions shown in blue are those that we selected for functional screening. \* indicates when the same amino acid substitution has been found in the 1000 Genome 1000 database <http://www.internationalgenome.org/home>, together with the number of subjects presenting with the same substitutions (n).

Supplementary Table 2. Screening missense mutations of GluN2B

Variant	Location	Glutamate potency ( $\mu\text{M}$ )	Current density (pA/pF)	$R_i$ ( $\text{M}\Omega$ )	Patient phenotype
WT	-	$7.18 \pm 0.82$	$-20.36 \pm 4.54$	$27.04 \pm 10.09$	-
C456Y	S1	-	-	-	Autism
C461F	S1	$511.4 \pm 55.49^{*****}$	$-6.49 \pm 3.94^{**}$	$36.44 \pm 32.53^a$	LGS with autistic features
R540H	S1-M1	$3.17 \pm 1.31^*$	$-30.31 \pm 7.71$	$18.86 \pm 6.22$	WS
P553L	Pre-M1	$12.67 \pm 2.01^*$	$-15.31 \pm 3.70$	<sup>b</sup>	Severe ID
N615I	M2-M3	$9.15 \pm 1.23$	$-19.19 \pm 3.24$	$1.33 \pm 0.15^{***}$	WS
V618G	M2-M3	$6.08 \pm 1.43$	$-17.55 \pm 3.35$	$1.46 \pm 0.99^{***}$	WS
A636P	M3	-	-	-	Mild ID
R682C	M3-S2	$8.64 \pm 1.22$	$-15.34 \pm 2.56$	$7.38 \pm 3.21$	Moderate ID
L825V	M4	$7.66 \pm 1.25$	$-19.06 \pm 3.65$	$17.99 \pm 4.20$	Autism

## Supplementary Table 2. Screening missense mutations of GluN2B

Functional and clinical parameters for nine GluN2B subunit missense mutations. These mutants were selected from Table 1 for screening of their functional properties by electrophysiology, following expression as GluN1-GluN2B diheteromers in HEK293 cells. Glutamate potency ( $\mu\text{M}$ ) is determined at  $-30\text{ mV}$  in the presence of  $10\ \mu\text{M}$  glycine and measured from the  $\text{EC}_{50}$ s from curve fits to glutamate concentration response curves. The glutamate current density ( $\text{pA/pF}$ ) is determined from the maximal glutamate current at  $-30\text{ mV}$  which is normalised to cell capacitance. The rectification index ( $R_i$ ) is measured from the current-voltage relationships in  $1.2\text{ mM Mg}^{2+}$  for responses induced by  $3\ \mu\text{M}$  glutamate and  $10\ \mu\text{M}$  glycine by determining the ratio of current evoked by glutamate at  $+60\text{ mV}$  /  $-60\text{ mV}$ . LGS – Lennox-Gastaut syndrome; WS - West syndrome; ID - intellectual disability.  $300\ \mu\text{M}$  glutamate was used for determining  $R_i$  due to the significant decrease in glutamate potency of receptors incorporating GluN2BC461F. <sup>b</sup>The I-V plot was not determined due to small steady-state currents. NMDARs containing GluN2BP553L resulted in pronounced desensitizing currents. No glutamate current was detected for GluN1-GluN2BC456Y and GluN1-GluN2BA636P up to  $3\text{ mM}$  glutamate. \*  $p < 0.05$ ; \*\*  $p < 0.01$ ; \*\*\*  $p < 0.005$ ; \*\*\*\*  $p < 0.001$ ; \*\*\*\*\*  $p < 0.0005$ ; \*\*\*\*\*  $p < 0.0001$ .

## Supplementary References

1. Tarabeux, J. *et al.* Rare mutations in N-methyl-D-aspartate glutamate receptors in autism spectrum disorders and schizophrenia. *Transl. Psychiatry* **1**, e55 (2011).
2. Endele, S. *et al.* Mutations in *GRIN2A* and *GRIN2B* encoding regulatory subunits of NMDA receptors cause variable neurodevelopmental phenotypes. *Nat. Genet.* **42**, 1021–1026 (2010).
3. Allen, A. S. *et al.* *De novo* mutations in epileptic encephalopathies. *Nature* **501**, 217–221 (2013).
4. Freunscht, I. *et al.* Behavioral phenotype in five individuals with *de novo* mutations within the *GRIN2B* gene. *Behav. Brain Funct.* **9**, 20 (2013).
5. de Ligt, J. *et al.* Diagnostic exome sequencing in persons with severe intellectual disability. *N. Engl. J. Med.* **367**, 1921–1929 (2012).
6. Roak, B. J. O. *et al.* Multiplex targeted sequencing identifies recurrently mutated genes in autism spectrum disorders. *Science* **23**, 1619–1623 (2012).
7. Lemke, J. R. *et al.* *GRIN2B* mutations in West syndrome and intellectual disability with focal epilepsy. *Ann. Neurol.* **75**, 147–154 (2014).
8. O’Roak, B. J. *et al.* Exome sequencing in sporadic autism spectrum disorders identifies severe *de novo* mutations. *Nat. Genet.* **43**, 585–589 (2011).